Research Article | Vol. 25, No. 7 | 3 Apr 2017 | OPTICS EXPRESS 7859

Optics EXPRESS

Test of mode-division multiplexing and demultiplexing in free-space with diffractive transformation optics

GIANLUCA RUFFATO,[1,2,*] MICHELE MASSARI,[1,2] GIUSEPPE PARISI,[3] AND FILIPPO ROMANATO[1,2,4]

[1]*Department of Physics and Astronomy 'G. Galilei', University of Padova, via Marzolo 8, 35131 Padova, Italy*
[2]*Laboratory for Nanofabrication of Nanodevices, c.so Stati Uniti 4, 35127 Padova, Italy*
[3]*SM Optics – SIAE Group, Via M. Buonarroti 21, 20093 Cologno Monzese, Milano, Italy*
[4]*CNR -INFM TASC IOM National Laboratory, S.S. 14 Km 163.5, 34012 Basovizza, Trieste, Italy*
[*]*gianluca.ruffato@unipd.it*

Abstract: In recent years, mode-division multiplexing (MDM) has been proposed as a promising solution in order to increase the information capacity of optical networks both in free-space and in optical fiber transmission. Here we present the design, fabrication and test of diffractive optical elements for mode-division multiplexing based on optical transformations in the visible range. Diffractive optics have been fabricated by means of 3D high-resolution electron beam lithography on polymethylmethacrylate resist layer spun over a glass substrate. The same optical sequence was exploited both for input-mode multiplexing and for output-mode sorting after free-space propagation. Their high miniaturization level and efficiency make these optical devices ideal for integration into next-generation platforms for mode-division (de)multiplexing in telecom applications.

OCIS codes: (050.1970) Diffractive optics; (050.4865) Optical vortices; (060.4510) Optical communications; (110.6895) Three-dimensional lithography.

References and links

1. E. Agrell, M. Karlsson, A. R. Chraplyvy, D. J. Rochardson, P. M. Krummrich, P. Winzer, K. Roberts, J. K. Fisher, S. J. Savory, B. J. Eggleton, M. Secondini, F. R. Kschischang, A. Lord, J. Prat, I. Tomkos, J. E. Bowers, S. Srinivasan, M. B. Pearce, and N. Gisin, "Roadmap of optical communications," J. Opt. **18**(6), 063002 (2016).
2. S. Yu, "Potentials and challenges of using orbital angular momentum communications in optical interconnects," Opt. Express **23**(3), 3075–3087 (2015).
3. L. Allen, M. W. Beijersbergen, R. J. C. Spreeuw, and J. P. Woerdman, "Orbital angular momentum of light and the transformation of Laguerre-Gaussian laser modes," Phys. Rev. A **45**(11), 8185–8189 (1992).
4. D. L. Andrews and M. Babiker, *The Angular Momentum of Light* (Cambridge University, 2013).
5. J. Wang, J.-Y. Yang, I. M. Fazal, N. Ahmed, Y. Yan, H. Huang, Y. Ren, Y. Yue, S. Dolinar, M. Tur, and A. E. Willner, "Terabit free-space data transmission employing orbital angular momentum multiplexing," Nat. Photonics **6**(7), 488–496 (2012).
6. F. Tamburini, E. Mari, A. Sponselli, B. Thidé, A. Bianchini, and F. Romanato, "Encoding many channels on the same frequency through radio vorticity: first experimental test," New J. Phys. **14**(3), 033001 (2012).
7. N. Bozinovic, Y. Yue, Y. Ren, M. Tur, P. Kristensen, H. Huang, A. E. Willner, and S. Ramachandran, "Terabit-scale orbital angular momentum mode division multiplexing in fibers," Science **340**(6140), 1545–1548 (2013).
8. A. Trichili, C. Rosales-Guzmán, A. Dudley, B. Ndagano, A. Ben Salem, M. Zghal, and A. Forbes, "Optical communication beyond orbital angular momentum," Sci. Rep. **6**(1), 27674 (2016).
9. M. Mirhosseini, O. S. Magana-Loaiza, M. N. O'Sullivan, B. Rudenburg, M. Malik, M. P. J. Lavery, M. J. Padgett, D. J. Gauthier, and R. W. Boyd, "High-dimensional quantum cryptography with twisted light," New J. Phys. **17**(3), 033033 (2015).
10. J. Leach, M. J. Padgett, S. M. Barnett, S. Franke-Arnold, and J. Courtial, "Measuring the orbital angular momentum of a single photon," Phys. Rev. Lett. **88**(25), 257901 (2002).
11. G. C. G. Berkhout, M. P. J. Lavery, J. Courtial, M. W. Beijersbergen, and M. J. Padgett, "Efficient sorting of orbital angular momentum states of light," Phys. Rev. Lett. **105**(15), 153601 (2010).
12. M. P. J. Lavery, D. J. Robertson, G. C. G. Berkhout, G. D. Love, M. J. Padgett, and J. Courtial, "Refractive elements for the measurement of the orbital angular momentum of a single photon," Opt. Express **20**(3), 2110–2115 (2012).

#283233 https://doi.org/10.1364/OE.25.007859
Journal © 2017 Received 19 Dec 2016; revised 10 Mar 2017; accepted 10 Mar 2017; published 28 Mar 2017

Optics EXPRESS

13. M. P. J. Lavery, D. J. Robertson, A. Sponselli, J. Courtial, N. K. Steinhoff, G. A. Tyler, A. E. Wilner, and M. J. Padgett, "Efficient measurement of an optical orbital-angular-momentum spectrum comprising more than 50 states," New J. Phys. **15**(1), 013024 (2013).
14. M. N. O'Sullivan, M. Mirhosseini, M. Malik, and R. W. Boyd, "Near-perfect sorting of orbital angular momentum and angular position states of light," Opt. Express **20**(22), 24444–24449 (2012).
15. M. Mirhosseini, M. Malik, Z. Shi, and R. W. Boyd, "Efficient separation of the orbital angular momentum eigenstates of light," Nat. Commun. **4**, 2781 (2013).
16. H. Huang, G. Milione, M. P. J. Lavery, G. Xie, Y. Ren, Y. Cao, N. Ahmed, T. An Nguyen, D. A. Nolan, M.-J. Li, M. Tur, R. R. Alfano, and A. E. Willner, "Mode division multiplexing using an orbital angular momentum mode sorter and MIMO-DSP over a graded-index few-mode optical fibre," Sci. Rep. **5**, 14931 (2015).
17. R. Fickler, R. Lapkiewicz, M. Huber, M. P. J. Lavery, M. J. Padgett, and A. Zeilinger, "Interface between path and orbital angular momentum entanglement for high-dimensional photonic quantum information," Nat. Commun. **5**, 4502 (2014).
18. K. S. Morgan, I. S. Raghu, and E. G. Johnson, "Design and fabrication of diffractive optics for orbital angular momentum space division multiplexing," Proc. SPIE **9374**, 93740Y (2015).
19. P. Bierdz, M. Kwon, C. Roncaioli, and H. Deng, "High fidelity detection of the orbital angular momentum of light by time mapping," New J. Phys. **15**(11), 113062 (2013).
20. T. Su, R. P. Scott, S. S. Djordjevic, N. K. Fontaine, D. J. Geisler, X. Cai, and S. J. B. Yoo, "Demonstration of free space coherent optical communication using integrated silicon photonic orbital angular momentum devices," Opt. Express **20**(9), 9396–9402 (2012).
21. A. Belmonte and J. P. Torres, "Digital coherent receiver for orbital angular momentum demultiplexing," Opt. Lett. **38**(2), 241–243 (2013).
22. V. V. Kotlyar, S. N. Khonina, and V. A. Soifer, "Light field decomposition in angular harmonics by means of diffractive optics," J. Mod. Opt. **45**(7), 1495–1506 (1998).
23. G. Gibson, J. Courtial, M. Padgett, M. Vasnetsov, V. Pas'ko, S. Barnett, and S. Franke-Arnold, "Free-space information transfer using light beams carrying orbital angular momentum," Opt. Express **12**(22), 5448–5456 (2004).
24. N. Zhang, X. C. Yuan, and R. E. Burge, "Extending the detection range of optical vortices by Dammann vortex gratings," Opt. Lett. **35**(20), 3495–3497 (2010).
25. J. Zhou, W. Zhang, and L. Chen, "Experimental detection of high-order or fractional orbital angular momentum of light based on a robust mode converter," Appl. Phys. Lett. **108**(11), 111108 (2016).
26. W. Zhang, Q. Qi, J. Zhou, and L. Chen, "Mimicking Faraday Rotation to Sort the Orbital Angular Momentum of Light," Phys. Rev. Lett. **112**(15), 153601 (2014).
27. H. Zhou, D. Fu, J. Dong, P. Zhang, D. Chen, X. Cai, F. Li, and X. Zhang, "Orbital angular momentum complex spectrum analyzer for vortex light based on the rotational Doppler effect," Light Sci. Appl. **6**, e16251 (2017).
28. J. Wang, "Advances in communications using optical vortices," Photon. Res. **4**(5), B14–B28 (2016).
29. G. Labroille, B. Denolle, P. Jian, P. Genevaux, N. Treps, and J.-F. Morizur, "Efficient and mode selective spatial mode multiplexer based on multi-plane light conversion," Opt. Express **22**(13), 15599–15607 (2014).
30. S. Gao, T. Lei, Y. Li, Y. Yuan, Z. Xie, Z. Li, and X. Yuan, "OAM-labeled free-space optical flow routing," Opt. Express **24**(19), 21642–21651 (2016).
31. T. Lei, M. Zhang, Y. Li, P. Jia, G. N. Liu, X. Xu, Z. Li, C. Min, J. Lin, C. Yu, H. Niu, and X. Yuan, "Massive individual orbital angular momentum channels for multiplexing enabled by Dammann gratings," Light Sci. Appl. **4**(3), e257 (2015).
32. G. Milione, M. P. J. Lavery, H. Huang, Y. Ren, G. Xie, T. A. Nguyen, E. Karimi, L. Marrucci, D. A. Nolan, R. R. Alfano, and A. E. Willner, "4 × 20 Gbit/s mode division multiplexing over free space using vector modes and a q-plate mode (de)multiplexer," Opt. Lett. **40**(9), 1980–1983 (2015).
33. Y. Yan, Y. Yue, H. Huang, J. Y. Yang, M. R. Chitgarha, N. Ahmed, M. Tur, S. J. Dolinar, and A. E. Willner, "Efficient generation and multiplexing of optical orbital angular momentum modes in a ring fiber by using multiple coherent inputs," Opt. Lett. **37**(17), 3645–3647 (2012).
34. B. Guan, R. P. Scott, C. Qin, N. K. Fontaine, T. Su, C. Ferrari, M. Cappuzzo, F. Klemens, B. Keller, M. Earnshaw, and S. J. B. Yoo, "Free-space coherent optical communication with orbital angular, momentum multiplexing/demultiplexing using a hybrid 3D photonic integrated circuit," Opt. Express **22**(1), 145–156 (2014).
35. B. J. Wiley, D. Qin, and Y. Xia, "Nanofabrication at high throughput and low cost," ACS Nano **4**(7), 3554–3559 (2010).
36. G. Ruffato, M. Massari, and F. Romanato, "Diffractive optics for combined spatial- and mode- division demultiplexing of optical vortices: design, fabrication and optical characterization," Sci. Rep. **6**(1), 24760 (2016).
37. M. Massari, G. Ruffato, M. Gintoli, F. Ricci, and F. Romanato, "Fabrication and characterization of high-quality spiral phase plates for optical applications," Appl. Opt. **54**(13), 4077–4083 (2015).
38. C. Wan, J. Chen, and Q. Zhan, "Compact and high-resolution optical orbital angular momentum sorter," APL Photonics **2**(3), 031302 (2017).
39. G. Ruffato, M. Massari, and F. Romanato, "Compact sorting of optical vortices by means of diffractive transformation optics," Opt. Lett. **42**(3), 551–554 (2017).

Optics EXPRESS

1. Introduction

In the last decades, several methods have been presented in order to deal with the growing worldwide demand of bandwidth and to boost the information capacity of optical networks [1]. Basically, almost all these techniques were about the manipulation of different physical dimensions of light waves, including frequency/wavelength, time, complex amplitude and polarization. More recently, the attention has been focused on the spatial degree of freedom, in the so-called spatial division multiplexing (SDM), consisting in tailoring the spatial structure and distribution of the transmitted waves. Mode-division multiplexing (MDM), in particular, is aimed at exploiting the several orthogonal modes supported by the transmission medium as distinct information channels. The axial symmetry of optical fibers and, obviously, of free-space, suggests the selection of modes carrying orbital angular momentum (OAM) of light as possible candidates [2]. These modes are characterized by a helical phase form $\exp(i\ell\varphi)$ ($\ell = 0, \pm 1, \pm 2,\ldots$), being ℓ the topological charge and φ the azimuthal coordinate [3,4]. Beams carrying different OAM are intrinsically orthogonal and separable from each other. The exploitation of OAM modes has demonstrated to allow promising results both in free-space [5,6] and in optical fiber transmission [7], either as distinct information channels or as high-dimensional alphabet for classical [8], and quantum applications [9].

The crucial parts of an optical link based on MDM are represented by the multiplexer and the demultiplexer, that is by the optical techniques exploited to prepare a collimated superposition of modes at the transmitter and to separate them at the receiver, respectively. Different solutions have been presented and described in order to sort a set of multiplexed beams differing in their OAM content: interferometric methods [10], optical transformations [11–18], time-division technique [19], integrated silicon photonics [20], coherent detection [21], OAM-mode analyzers [22–24], astigmatic-mode conversion [25], rotational Doppler effect [26,27].

These methods are commonly presented and considered for demultiplexing operations, and multiplexing is only marginally demonstrated by invoking the invariance of the light path for time-reversal [28]. Therefore, very little attention has been devoted in literature to the multiplexing process, which is usually performed with cumbersome beam-splitters, in a lossy and non-scalable manner. Recently, mode multiplexers based on multiplane light conversion [29], complex phase mask and gratings [30,31], *q*-plates [32], fiber and photonic integrated devices [33,34] have been proposed as promising candidates for optical vortex multiplexing.

Here we consider the sorting technique based on transformation optics and we test, in sequence, the same configuration for both multiplexing and demultiplexing of OAM beams in free-space at $\lambda = 632.8$ nm. In order to increase the compactness of the sorting scheme, we realized the optical elements in a diffractive form, i.e. their phase function has been lithographically patterned in the form of a modulo-2π relief. This realization avoids bulky refractive elements and provides a higher miniaturization level, especially when short focal lengths are required. Samples have been fabricated with electron-beam lithography (EBL) on polymethylmethacrylate resist layer, spun over a glass substrate, in high-resolution mode with 5-nm resolution, providing high-quality phase-only diffractive optical elements. Then the possibility to replicate the fabricated optics with fast mass-production techniques, such as nano-imprint lithography [35], which allows high throughput and much lower production costs, makes these optical elements promising for integration into optical platforms for MDM.

2. OAM-mode division multiplexing with transformation optics

Demultiplexing solutions based on transformation optics demonstrated how OAM states can be efficiently converted into transverse momentum states through a *log-pol* optical transformation [11]. Two elements are strictly necessary: the unwrapper and the phase-corrector. The former performs the conformal mapping of a position (x, y) in the input plane

Optics EXPRESS

to a position (u, v) in the output plane, where $v = a \arctan(y/x)$ and $u = -a \ln(r/b)$, with $r = (x^2 + y^2)^{1/2}$, being a and b design parameters. Its phase function Ω_1 is given by:

$$\Omega_1(x,y) = \frac{2\pi a}{\lambda f_1}\left[y \arctan\left(\frac{y}{x}\right) - x \ln\left(\frac{\sqrt{x^2+y^2}}{b}\right) + x + \frac{x^2+y^2}{2a}\right] \quad (1)$$

where the two free parameters a and b determine the scaling and position of the transformed beam, respectively. The parameter a takes the value $L/2\pi$, ensuring that the azimuthal angle range $(0, 2\pi)$ is mapped onto a length L which is shorter than the full width of the second element. The parameter b is optimized for the particular physical dimensions of the sorter and can be chosen independently. The phase-corrector, placed at a distance f_1, has a phase function Ω_2 given by:

$$\Omega_2(u,v) = -\frac{2\pi ab}{\lambda f_1}\exp\left(-\frac{u}{a}\right)\cos\left(\frac{v}{a}\right) \quad (2)$$

A lens with focal length f_2 is inserted after the phase-corrector element in order to focus the transformed beam onto a specified lateral position, which moves proportionally to the OAM content ℓ according to:

$$\Delta s = \frac{f_2 \lambda}{2\pi a}\ell \quad (3)$$

Alternatively, the focusing quadratic term can be integrated in the phase-corrector element as well.

The same setup has been demonstrated to work as multiplexer, in reverse. In this case the two elements are illuminated in the opposite direction. The input beam should be properly reshaped into an asymmetric elongated spot which is wrapped by the first element (phase-corrector) and then corrected in its phase by the second element (unwrapper). Thus the azimuthal phase gradient of the output beam is achieved by wrapping the input linear phase gradient, which is in turn obtained by illuminating the first element with a non-null incidence angle. In [17] for instance, this was obtained by using the diffraction pattern of an axially-shifted slit.

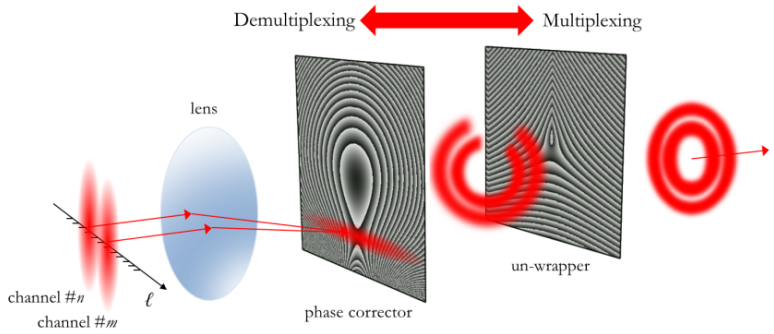

Fig. 1. Schematic of the (de)multiplexer working principle. From left to right: multiplexing. The input beam should be reshaped into an elongated form, for instance using a cylindrical lens. Then it is Fourier-transformed with a lens and it illuminates the first optical element with a tilted angle, depending on the initial axial displacement with respect to the axis of the lens. Then the beam is wrapped and illuminates the second optical element for phase correction. The system converts an input linear phase gradient, created by the tilted incidence, into an output azimuthal phase gradient. Beams with different axial displacements in input are converted into beams with different OAM content. From right to left: demultiplexing.

Here we propose a more efficient technique, similar to the one exploited in [16], consisting in reshaping a Gaussian beam with a cylindrical lens and using a spherical lens in

Optics EXPRESS

f-f configuration to convert the axial displacement of the input beam into a tilted one, thanks to Fourier transform properties (Fig. 1). As far as fabrication is concerned, in its first realization the two elements were implemented with spatial light modulators (SLMs) [11]. At a later stage [12], they were replaced by two freeform refractive optical components, exhibiting higher efficiency, though not a small size. In this work, we further improve the miniaturization level by realizing them in a diffractive form with 256 phase levels.

3. Fabrication and optical characterization

3.1 Electron beam lithography

Diffractive optical elements are fabricated as surface-relief patterns of pixels. This 3-D structure can be realized by shaping a layer of transparent material, imposing a direct proportionality between the thickness of the material and the phase delay. By using the correlation between the dosage level and the final structure height, it is possible to convert the dosage spatial distribution to the final geometry. Electron beam lithography (EBL) has been demonstrated to have distinguished performance in creating diffractive optical elements, due to the possibility to realize 3D digital and continuous surface profiles, high flexibility in the elements design, and remarkable optical quality of the fabricated reliefs [36,37].

In this work, the DOE patterns were written on a polymethylmethacrylate (PMMA) resist layer with a JBX-6300FS JEOL EBL machine, 12 MHz, 5 nm resolution, working at 100 keV with a current of 100 pA, by means of a proximity-effect correction assisted ultra-fine process. The substrate used for the fabrication is glass coated with an ITO layer with conductivity of 8-12 Ω, in order to ensure both transparency and a good discharge during the exposure. Coating the resist with a thin layer of gold allowed both to further reduce the beam charging and to exploit the JBX-6300FS white light height detection system, useless for transparent substrates. By measuring a height map of the surface, this system offers advantages both in stitching removal and in pattern resolution, thanks to a more precise setting of the beam focus. Patterned samples were developed under slight agitation in a temperature-controlled developer bath for 60 s in a solution of deionized water: isopropyl alcohol (IPA) 3:7.

For the working wavelength λ = 632.8nm, the PMMA refractive index results n_{PMMA} = 1.489 from spectroscopic ellipsometry analysis (J.A. Woollam VASE, 0.3 nm spectral resolution, 0.005° angular resolution). The height d_k of the pixel belonging to the kth layer is given by:

$$d_k = \frac{\lambda}{n_{PMMA} - 1} \frac{k-1}{N} \tag{4}$$

being N the number of phase levels. In our case of interest, for N = 256 we get: d_1 = 0 nm, d_{256} = 1289.4 nm, step Δd = 5.1 nm. In Fig. 2 fabricated samples are shown, with design parameters f_1 = 9 mm, a = 220 μm, b = 50 μm. A tilt term was added to the phase-corrector in the demultiplexing sequence, with carrier spatial frequencies $\alpha = \beta$ = 0.1 μm^{-1}, in order to prevent any overlap on the CCD with the potentially noise-carrier zero-order term.

Optics EXPRESS

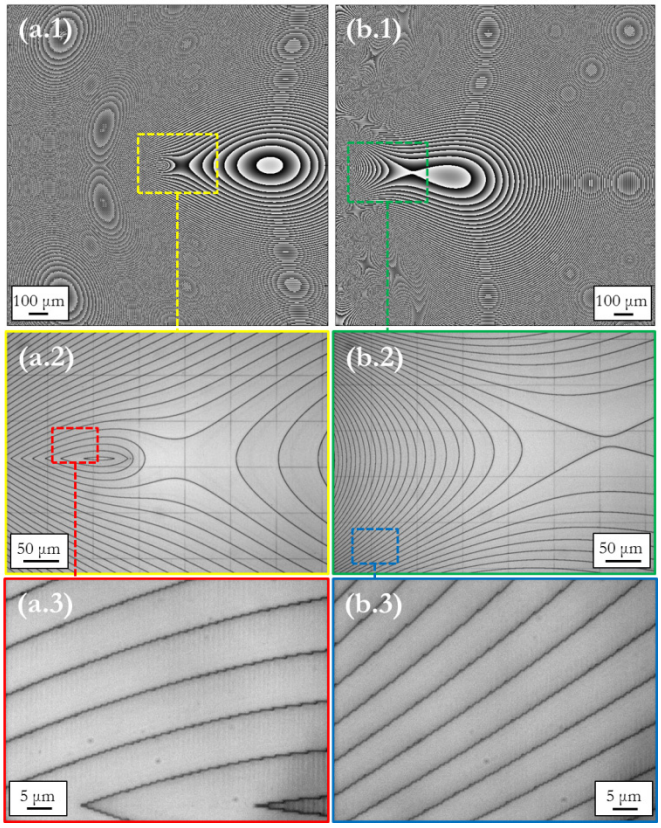

Fig. 2. Diffractive optics for *log-pol* coordinate transformation. Computed phase patterns (a.1, b.1), optical microscope inspections and details: unwrapper (a.1, a.2, a.3) and phase-corrector (b.1, b.2, b.3). Design parameters: a = 220 µm, b = 50 µm, f_1 = 9 mm, carrier spatial frequency in the phase-corrector for image tilt (in the demultiplexer): $\alpha = \beta = 0.1$ µm^{-1}. Optimized for wavelength λ = 632.8 nm. 256 phase levels. Total size: 1.6 x 1.6 mm^2.

3.2 Optical characterization

The characterization setup was mounted on an optical table (Fig. 3). In order to prove the demultiplexing of beams carrying different values of OAM, we simulated an array of several laser sources by considering a single laser beam and translating it along a direction perpendicular to the propagation axis. In such a way, different positions of the laser correspond to different excited modes, i.e. different channels, and they are expected to be correctly sorted and detected at different positions after the demultiplexer.

The Gaussian beam (λ = 632.8 nm, beam waist w_0 = 240 µm, power 0.8 mW) emitted by a HeNe laser source (HNR008R, Thorlabs) is reshaped with a cylindrical lens in order to prepare an elongated input beam to be wrapped by the multiplexer. Both laser and reshaping lens are mounted on the same stage and can be translated together using a micrometric translator (TADC-651, Optosigma) in the direction orthogonal to the propagation direction. The transmitted beam is Fourier-transformed with a first lens of focal length f_0 = 75 mm, which is exploited to convert the axial displacement of the input beam into a tilted beam illuminating the first diffractive element (phase-corrector). For increasing laser shift, i.e. increasing angle of incidence on the multiplexer, beams with increasing OAM are generated. By translating the laser in opposite directions with respect to the $\ell = 0$ position, beams with opposite helicity are generated (Fig. 4). Both phase corrector and un-wrapper are mounted on a XY translation sample holder with micrometric drives for sample alignment. A beam-splitter is used to analyze the field profile, which is collected with a CCD camera

Optics EXPRESS

(DCC1545M, Thorlabs, 1280x1024 pixels, 5.2 μm pixel size, monochrome, 8-bit depth). Then the beam illuminates the demultiplexing sequence. Al last, the far-field is collected by a second CCD camera (1500M-GE, Thorlabs, 1392x1040 pixels, 6.45 μm pixel size, monochrome, 12-bit depth) placed at the back-focal plane of a lens of focal length f_2 = 10 cm. In far-field, a bright asymmetric spot appears whose position shifts linearly with the OAM content, i.e., with the laser lateral position (Fig. 4(d)). In Fig. 4(b) the output field is shown for an input beam corresponding to $\ell = -4$.

Subsequently, a further laser beam was added, placing a second beam-splitter before the multiplexing sequence (Fig. 3). The second laser is mounted on a linear translator as well, and its OAM content can be controlled independently from the first one. In Fig. 4(c) the two multiplexed beams are shown in case of $\ell = -5$ and $\ell = +5$ respectively. As expected, while the beams are superimposed after the multiplexer, two clearly separated signals appear after demultiplexing sequence.

A Mach-Zehnder interferometric setup was added in order to analyze the phase pattern of the modes generated by the multiplexing optics (Fig. 3). In Fig. 5, the intensity patterns and the corresponding interferograms are shown for six different laser positions with ℓ in the range from 0 to + 5. As expected, ℓ-fold fork dislocations appear in correspondence of the central dark singularity.

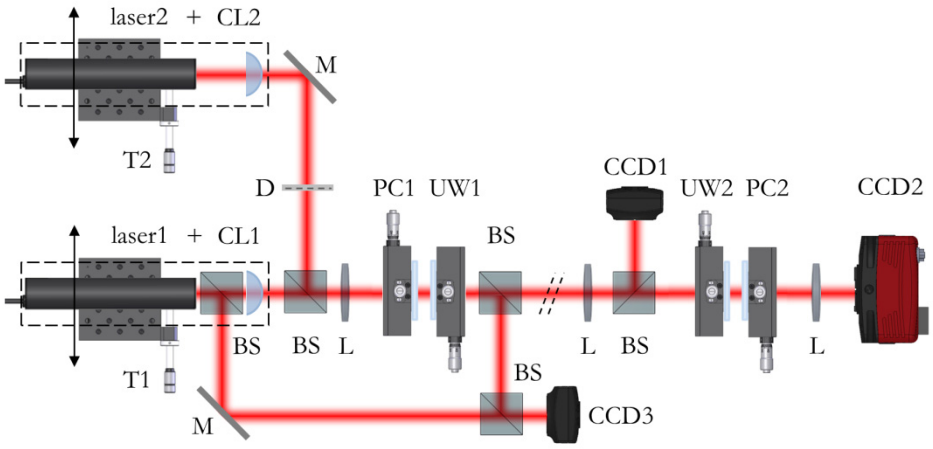

Fig. 3. Experimental setup for OAM sorting with diffractive optical elements (DOE) implementing transformation optics. A laser (laser1) illuminates a cylindrical lens (CL1) for input beam reshaping. The input system can move perpendicularly to the propagation direction with a micrometric translator (T1). Then the beam is Fourier transformed with a lens (L) and illuminates the sequence of optical elements PC1-UW1 performing multiplexing. After travelling in free-space, the generated vortex is split with a 50:50 beam-splitter (BS) for beam analysis with a first camera (CCD1). The second part of the beam enters the demultiplexing sequence UW2-PC2. Finally, the beam is Fourier-transformed by a lens (L) and collected on a second camera (CCD2). A second input chain (laser2, CL2, T2) was added for the test of two-channel mode-division multiplexing. An iris diaphragm (D) can exclude this second beam. A third camera (CCD3) collects the interference pattern between the output laser beam and the output mode of the multiplexer (PC1-UW1) for the analysis of phase-pattern dislocations. For this purpose, additional beam-splitters and mirrors (M) are inserted for the design of the required Mach-Zehnder optical setup.

Optics EXPRESS

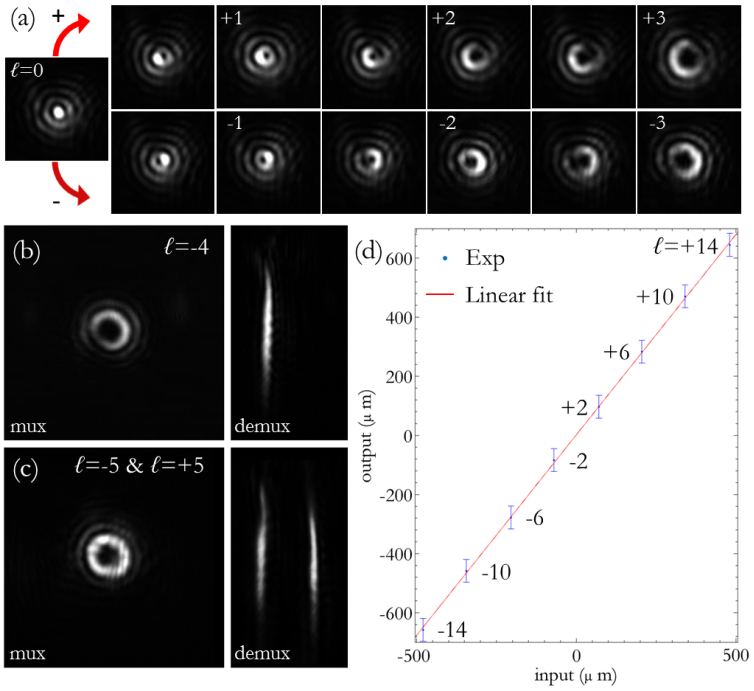

Fig. 4. (a) Images recorded with a CCD camera are shown for various OAM states up to the 3rd order (white numbers), for translation of the laser towards opposite directions. The distance between the lateral positions of the laser that generate integer OAM states was around 35 μm. In between these positions, fractional OAM modes are generated. (b) Generation and detection of a beam corresponding to $\ell = -4$. (c) Multiplexing and demultiplexing of two beams corresponding to $\ell = +5$ and $\ell = -5$. (d) Output position as a function of input laser shift, experimental data for ℓ in the range $\{-14,\ldots,+14\}$, step $\Delta\ell = 4$.

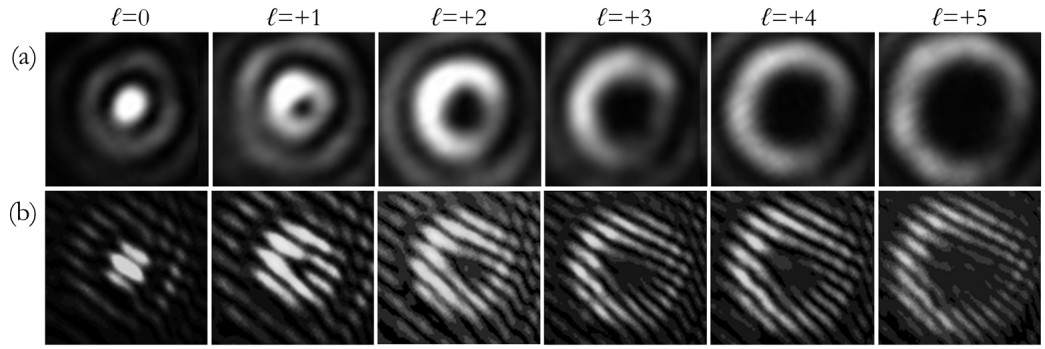

Fig. 5. Generated beams (a) and related interferograms (b) for input laser positions corresponding to OAM values from $\ell = 0$ to $\ell = 5$. Central fork-dislocations confirm the presence of a phase singularity along the axis of the beam.

4. Results and discussion

The CCD illuminated area is split into rectangular regions which are centered on each elongated spot in far-field with a size corresponding to the minimum separation between any two adjacent channels. By measuring the total intensity in each of these regions, we can determine the relative fraction of a specific OAM state in the input beam. We defined 29 of these regions, and we analyzed the optical response under illumination with pure vortices, generated by subsequently moving the input laser to positions corresponding to ℓ values

Optics EXPRESS

spanning in the range from $\ell = -14$ to $\ell = +14$. For each position of the laser, the beam impinges on the multiplexer with a different incidence angle and generates a different output mode, as described in the previous section.

As highlighted elsewhere [11–13], a limitation of OAM-beam sorting with *log-pol* transformation is represented by the slightly overlap between adjacent channels, which results into detrimental inter-channel cross-talk. One option for improvement is to include a fan-out element and its corresponding phase-corrector [14, 15], which extend the phase gradient by introducing multiple copies, thus providing a larger separation between spots, at the expense of increased complexity and size of the optical system. More recently the fan-out element has been integrated in the unwrapper [38], however a dual-phase corrector is required. Alternatively, the choice of non-consecutive OAM values can further diminish channel cross-talk, maintaining the same optical configuration with the original unwrapper and phase-corrector. With such a choice, the intensity spots in far-field result more separated and the overlap between adjacent channels is consequently reduced [39].

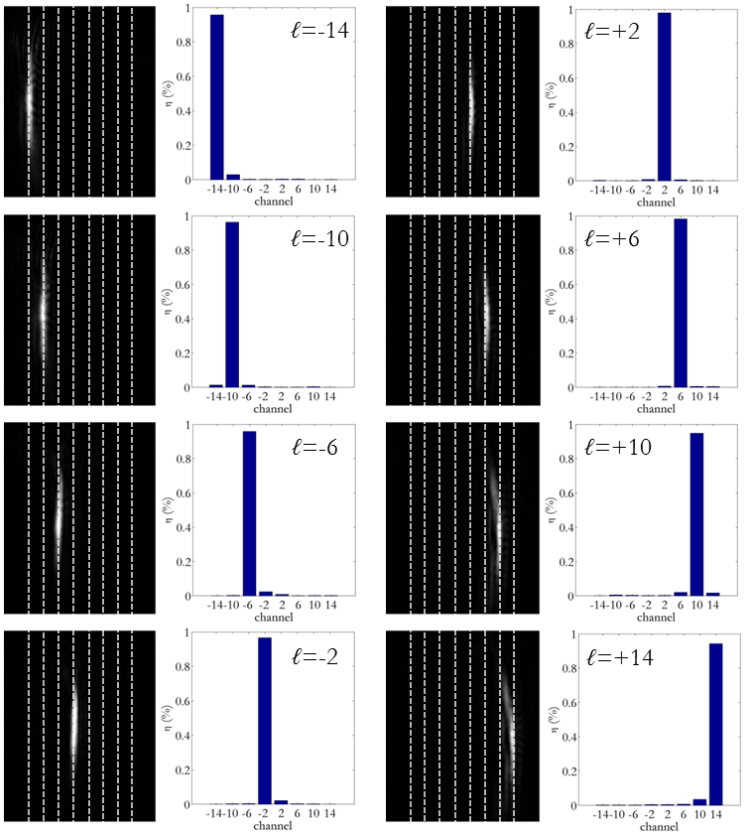

Fig. 6. Experimental intensity output and efficiency for 8 input modes, in the range $\ell = \{-14,\ldots,+14\}$, step $\Delta\ell = 4$. Bar-plot: channels efficiency.

The cross-talk XT on the channel $\ell = \ell^*$ is defined as:

$$XT_{\ell=\ell^*} = 10 \cdot \log_{10} \frac{I_{\ell^*,ALL\setminus\ell^*}}{I_{\ell^*,ALL}} \tag{5}$$

where $I_{\ell^*,ALL}$ is the signal in correspondence of channel ℓ^* when all input OAM signals in the set $\{\ell_i\}$ are on, ℓ^* included, while $I_{ALL\setminus(\ell^*)}$ is the signal at channel ℓ^* when the input channel

Optics EXPRESS

ℓ^* is off. The choice of $\Delta\ell = 4$ provides a good separation of far-field spots with channel efficiencies up to 94% and values lower than 4% for off-diagonal terms (Figs. 6 and 7(a)) and allows obtaining acceptable cross-talk values below −15 dB (Fig. 7(b)). The separation between consecutive spots is around 180.6 μm, close to the theoretical value 183.2 μm calculated with Eq. (3).

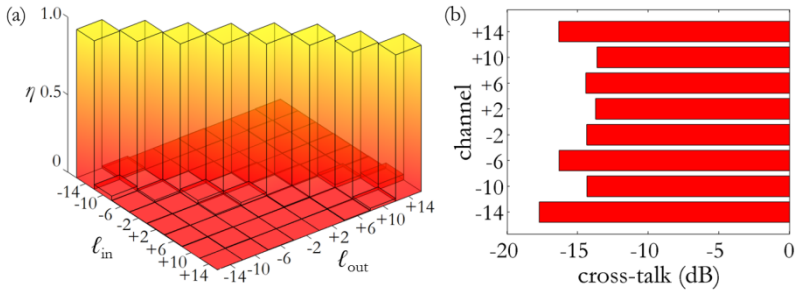

Fig. 7. Efficiency (a) and cross-talk (b) for 8 channels in the set {-14, …, + 14}, step $\Delta\ell = 4$.

5. Conclusions

We fabricated phase-only diffractive optical elements with high-resolution electron beam lithography and we demonstrated their performance for mode-division multiplexing based on transformation optics. The fabricated elements were integrated into a prototypal free-space optical link and the multiplexing and demultiplexing optical processes were tested and demonstrated using the same optical sequence, in reverse. By properly choosing design parameters and channel set, cross-talk values below −15 dB can be achieved. In a later step, samples fabricated by EBL can be replicated with fast mass-production techniques such as nano-imprint lithography, accomplishing the goal of producing high-throughput, low-cost and high-resolution optical elements. Thanks to the high efficiency and miniaturization level, the fabricated optics are promising for integration into optical platforms performing optical processing of OAM channels, also for applications in optical fibers.

Acknowledgments

This work was supported by SM Optics – SIAE Group. The authors gratefully thank Pierangelo Chiappa, Mauro Zontini, Romano Valussi and Alberto Mascetti for the interesting discussions.